Marín-Martínez, S.; Martínez Pérez, JD.; Valero, CI.; Boria Esbert, VE. (2017). Microstrip Filters with Enhanced Stopband Based on Lumped Bisected Pi-Sections with Parasitics. IEEE Microwave and Wireless Components Letters. 27(1):19-21. doi:10.1109/LMWC.2016.2630841

Microstrip Filters With Enhanced Stopband Based on Lumped Bisected Pi-Sections With Parasitics

Sandra Marín, Jorge D. Martínez, *Member, IEEE*, Clara I. Valero, and Vicente E. Boria, *Senior Member, IEEE*

***Abstract*— A procedure for improving the stopband response of planar bandpass filters is presented in this letter. The technique is based on the introduction of transmission zeros by using lumped-element bisected-pi sections at the filter input/output. As an example, a 3−pole 10% FBW bandpass filter with Chebyshev response centered at 1 GHz, based on strongly loaded combline microstrip resonators has been designed, manufactured and measured. The proposed solution can be used on any planar topology in order to improve the stopband performance with a negligible additional footprint.**

***Index Terms*— Lumped elements, microstrip filter, transmission zeros, ultra-wide stopband.**

I. Introduction

A WIDE spurious-free band is a common requirement in bandpass filters to be used for suppression of spurious outputs and image rejection in up/down-conversion applications. A high rejection level up to 3 – 7 times the passband center frequency f_0 is usually required in filters operating at intermediate frequencies (IFs) between 1–4 GHz.

Unfortunately, microstrip filters generally present spurious passbands at multiples of the design frequency. Even if some well-known topologies can help to improve the out-of-band response (e.g., interdigital or combline filters) it is still complicated to meet the former requirements. Therefore, several methods have been proposed in the literature to address this issue, e.g., by modifying the filter structure for integrating low-pass [1] or bandstop [2] responses, by loading coupled-line [3] and open-loop [4] filters with open-stubs, by controlling the resonator couplings to achieve multi-spurious rejection [5], or by introducing TZs within the filter stopband [6], [7].

In this letter, a simple but general technique for the introduction of TZs in a microstrip filter stopband is proposed by introducing lumped bisected $\pi-$sections (BPS) at the filter input and output. Each section will generate 2 independently-adjustable TZs due to the shunt and parasitic self-resonance frequency (SRF) of the lumped components, while presenting a good match within the filter passband. The additional footprint of these sections is almost negligible, and the technique is of broad application independently of the filter topology.

This work was supported in part by MINECO (Spanish Government) under project TEC2013-48036-C3-3-R and TEC2013-47037-C5-1-R.

S. Marín, J. D. Martínez, and V. E. Boria are with the Universitat Politécnica de Valéncia, 46022 Valéncia, Spain.

C. I. Valero is with Sistelbanda S.A., 46980 Valéncia, Spain.

Color versions of one or more of the figures in this paper are available

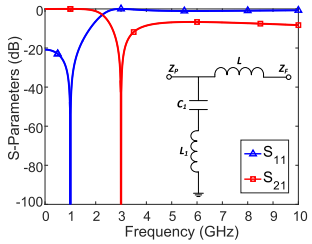

Fig. 1. Circuit schematic of the ideal bisected $\pi-$section and S-parameters response for $f_{TZ} = 3$ GHz, $f_0 = 1$ GHz, $Z_F = 50\ \Omega$ and $Z_P = 60\ \Omega$. ($L = 3.6$ nH, $C_1 = 1$ pF and $L_1 = 2.7$ nH).

II. Theory

A. Ideal Bisected $\pi-$ Section (BPS)

The circuit scheme of the proposed BPS cell is shown in Fig. 1. This network presents a low-pass response due to the series inductor L while introducing an adjustable transmission zero at the upper stopband of the filter.

The cascaded connection of this cell with the filter has to be done under certain matching conditions to keep the filter in-band return losses, but placing at the same time the TZ at the desired frequency.

Forcing the matching condition between the port impedance Z_P and the cell load (i.e., the filter impedance Z_F) at some frequency ω_0, and applying the series-parallel transformation to the BPS network, we can obtain the values of L, C_1 and L_1 from the following expressions:

$$L = \frac{Z_F\sqrt{\frac{Z_P}{Z_F}-1}}{\omega_0} \tag{1}$$

$$C_1 = \frac{\omega_{TZ}^2-\omega_0^2}{\omega_{TZ}^2\omega_0}\cdot\frac{1}{\omega_0 L\left(1+\left(\frac{Z_F}{\omega_0 L}\right)^2\right)} \tag{2}$$

$$L_1 = \frac{1}{\omega_{TZ}^2 C_1} \tag{3}$$

As the series matching element must be placed next to the termination with smallest resistance, we shall assume that $Z_P > Z_F$ in (1) without loss of generality.

This set of equations establishes the circuit values in terms of ω_{TZ}, ω_0, Z_F and Z_P. The theoretical response of the proposed network with $f_{TZ} = 3$ GHz, $f_0 = 1$ GHz, $Z_F = 50\ \Omega$ and $Z_P = 60\ \Omega$ can be seen in Fig. 1.

B. Lumped Bisected $\pi-$ Section With Parasitics

Lumped and/or quasi-lumped elements can be good candidates for implementing the proposed cell. Regarding lumped

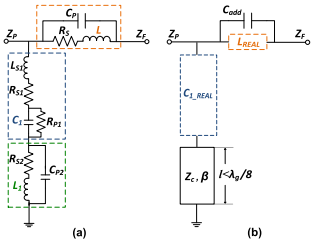

Fig. 2. Lumped bisected π - section. (a) Equivalent circuit of the real lumped elements of the network. (b) Modified lumped bisected π - section.

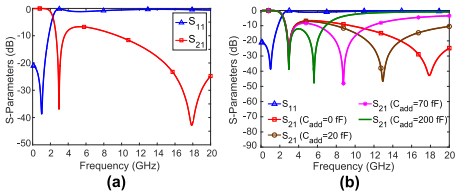

Fig. 3. Transmission and reflection characteristics of the lumped bisected π - sections with parasitics. (a) Real lumped elements cell. (b) Tunability of the second TZ vs different values of C_{add}.

components, they allow further miniaturization, do not show periodicity within the operating frequency range, and as will be demonstrated they enable us to introduce additional TZs due to the series self-resonance of the inductor L. Thus, it would be interesting to consider the real equivalent model where parasitics are included, as illustrated in Fig. 2 (a).

Analyzing the influence of the SRF of each lumped component, it is obvious that the series inductance L and the shunt capacitor C_1 are the elements that can introduce additional TZs in the response due to each component self-resonance. Thus, the series inductor L would generate an additional TZ at a finite frequency depending on its parasitic capacitance value C_P. On the contrary, no additional TZ would be produced by the shunt capacitor, due to the absorption of the parasitic inductance L_{S1} into the shunt inductor L_1.

Therefore, even if the self-resonance phenomenon of lumped elements is usually a drawback in most RF and microwave circuits, it can be used in BPS cells to improve the filter stopband. In order to control the location of this TZ, an additional capacitor C_{add} is added in parallel with the inductance as shown in Fig. 2 (b). The SRF of the series inductor L can be shifted to lower frequencies by increasing C_{add} value. A first value of the required capacitance can be obtained from the desired TZ frequency by taking into account the parasitic contribution C_P of the real inductor and the stray capacitance from the SMD assembly pads.

Finally, the shunt inductor L_1 can be easily implemented using a quasi-lumped short-circuited stub with $l << \frac{\lambda}{8}$. This is due to the low values required for this parameter when the TZ is located far from ω_0.

To demonstrate all the described effects, the ideal network of Fig. 1 has been simulated using commercial SMD components (*Coilcraft* - 0402 *HP* $L = 3.6$ nH and $L_1 = 2.7$ nH, and *AVX-Accu-P* 0402 C_1=*1* pF), and the results are presented in Fig. 3 (a). The response is similar to the theoretical one, since the matching and the TZ are maintained at 1 GHz and 3 GHz respectively, but a second TZ appears at 18 GHz originated from the SRF of the real inductance L. In this

TABLE I

FILTER SYNTHESIS AND LAYOUT VALUES

Parameter	Result	Layout Value
Z_a	65 Ω	3.5 mm
$\theta_0 = \beta l;\ l \approx \frac{\lambda_{g0}}{8}$	40^o	$l_1 = l_3 = 21.728$ mm; $l_2 = 20.728$ mm
$b = \frac{cot\theta_0 + \theta_0 csc^2\theta_0}{2Z_a}$	0.022	–
$C_d = \frac{cot\theta_0}{Z_a \omega_0}$	2.9 pF	2.2 pF 0402 AVX-Accu-P
$J_{01} = J_{34} = \sqrt{\frac{bFBW}{g_0 g_1 Z_A}}$	0.007	180 μm
$J_{12} = J_{23} = bFBW\sqrt{\frac{1}{g_1 g_2}}$	0.002	2.53 mm

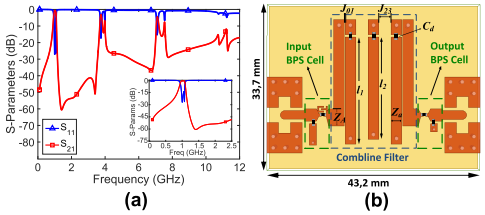

Fig. 4. (a) Simulation results of the microstrip bandpass filter. (b) Layout of the microstrip combline filter with two lumped bisected π - network.

TABLE II

FREQUENCY DISTRIBUTION OF TZS AND CELLS PARAMETERS RESULTS

Freq.	Method	Param. Values
$f_{TZ1} = 3$ GHz	Input section L-L_1-C_1	$L = 3.6$ nH $C_1 = 1.1$ pF $L_1 = 2.7$ nH
$f_{TZ2} = 3.85$ GHz	Output section L-L_1-C_1	$L = 3.6$ nH $C_1 = 1$ pF $L_1 = 1.5$ nH
$f_{TZ3} = 7$ GHz	SRF of L of Input section	$C_{add} = 150$ fF
$f_{TZ4} = 9.5$ GHz	SRF of L of Output section	$C_{add} = 80$ fF

context, the tuning of this second TZ with different values of C_{add} can also be observed in Fig. 3 (b), where small values of C_{add} are needed to shift this TZ in a wide range.

III. FILTER DESIGN

A. Strongly-Loaded Microstrip Combline Filter

The design goal is to implement a bandpass filter with a wide spurious-free band. It is well-known that in combline filters the frequency of the first spurious band can be controlled by a proper resonator design. Thereby, it is proposed a three-pole Chebyshev bandpass filter with 0.1 dB passband ripple and 10% FBW at a design frequency $f_0 = 1$ GHz, where its first spurious response should appear above $f > 2 \times f_0$ in order to have a moderately wide stopband.

The lowpass prototype coefficients of the former response are $g_0 = g_4 = 1$, $g_1 = g_3 = 1.0136$ and $g_2 = 1.1474$. Resonator and input/output port impedances are chosen as $Z_a = 65\ \Omega$ and $Z_A = 50\ \Omega$ respectively. Then, the resonator length is set slightly below $\lambda_{g0}/8$ by strongly loading the microstrip line using discrete capacitors, thus moving the first spurious band up to $4 \times f_0$. The required parameters of the filter (i.e., slope parameter b, lumped capacitance C_d and admittance inverter values $J_{i,i+1}$) can be obtained from the corresponding expressions shown in Table I.

Fig. 4 (a) shows the full-wave simulated filter performance. As expected, the first and second spurious band responses are

TABLE III

COMPARISON OF SOME ULTRA-WIDE STOP-BAND FILTERS IN PLANAR TECHNOLOGY

	Order	f_0(GHz)	FBW	IL(dB)	Harmonic Suppresion	Size(λ_g^2)	Topology	Technology
[1]	2nd	2.0	16%	1.1 dB	$2f_0 - 11.5f_0$ (−20 dB)	0.23×0.13	Shunt-Stubs	Multi-Layer Al_2O_3
[2]	7th	2.5	10%	2 dB	$1.1f_0 - 7f_0$ (−28 dB)	$\approx 2 \times 0.58$	Parallel-Coupled Lines	PCB Single-Layer
[3]	7th	1.0	20%	5.1 dB	$1.2f_0 - 10f_0$ (−35 dB)	1.70×0.70	Parallel-Coupled Lines	PCB Single-Layer
[4]	4th	1.0	4.8%	2.8 dB	$1.1f_0 - 12.2f_0$ (−30 dB)	0.47×0.15	Loaded Stubs	PCB Single-Layer
[5]	5th	2.0	10%	2.2 dB	$1.3f_0 - 7f_0$ (−25 dB)	0.15×0.45	Parallel-Coupled Lines	PCB Single-Layer
[6]	–	0.89	87%	0.7 dB	$1.6f_0 - 13.2f_0$ (−20 dB)	0.12×0.07	Cascaded LPF-HPF	PCB Single-Layer
[7]	4th	0.5	20%	3.5 dB	$1.2f_0 - 7f_0$ (−30 dB)	0.03×0.06	Lumped Element	Multi-Layer LCP
This work	3rd	1.0	10%	1.2 dB	$1.1f_0 - 10f_0$ (−22 dB)	0.18×0.16	Combline	PCB Single-Layer

approximately located at 4 and 7 GHz, providing a rejection higher than 25 dB up to $3.5 \times f_0$.

B. Filter With Four Transmission Zeros

Two lumped BPS cells are added to the designed filter structure, one at the input and the other at the ouput. In this manner, it is possible the introduction of four TZs at different frequencies to suppress the two additional undesirable spurious bands. To reach a rejection better than 30 dB until $10 \times f_0$, the frequency distribution of TZs has to be done adequately. Therefore, an optimization procedure combining the 3D EM simulation of the filter with the circuital models of the BPS cells has been performed. The proper location of the TZs and the corresponding element values are shown in Table II.

As the filter impedance $Z_F = Z_A$ is 50 Ω, the input/output port impedance Z_P is chosen as 60 Ω. The ratio $\frac{Z_P}{Z_F}$ must be a trade-off between matching bandwidth and practical implementation of filter and port impedances, as well as lumped-element values obtained. The BPS series inductors L_1 are implemented by short-circuited stubs of $Z_0 = 80.5\Omega$ and via diameter of 0.5 mm. The stub lengths are 4.4 mm and 1.65 mm for the input and output BPS cell, respectively. The TZs originated by the SRF of L are also influenced by the SMD package stray capacitance that has been estimated in $70 - 80$ fF using 3D EM simulations. Thus, no additional capacitance is needed at the output BPS cell, while a $C_{add} = 70\ fF$ is required at the input. An interdigital capacitor structure consisting on 3 fingers of 1.5 mm of length and equal 0.25 mm width and gap are used to reach this capacitance value. The layout of the complete filter is depicted in Fig. 4 (b). The occupied area is only 43x33 mm^2 for a 1 GHz filter. It should be remarked the negligible size increment ought to the insertion of both BPS cells.

IV. EXPERIMENTAL RESULTS

The filter has been fabricated in a 1.524 mm-thick Rogers RO4003C substrate ($\epsilon_r = 3.55$, $\tan\delta = 2.7 \cdot 10^{-3}$). A photography of the device is shown in Fig. 5. S-parameters results can be seen in Fig. 5, and are in very good agreement with the simulated values. The mid-band insertion losses are 1.2 dB, with return losses better than 13 dB within a 3-dB bandwidth of 12%. A rejection higher than 22 dB is obtained up to 10 GHz, providing an ultra-wide stopband even if a slight frequency shift of some TZs can be observed, due to the fabrication tolerances regarding the interdigital capacitor. A comparison with other ultra-wide stop-band filters is shown in Table III. As can be seen, the proposed solution achieves state-of-the art performance while being completely independent of the filter topology, with a minimal footprint on the design, and introducing up to 4 independently adjustable TZs for suppresing the first spurious bands.

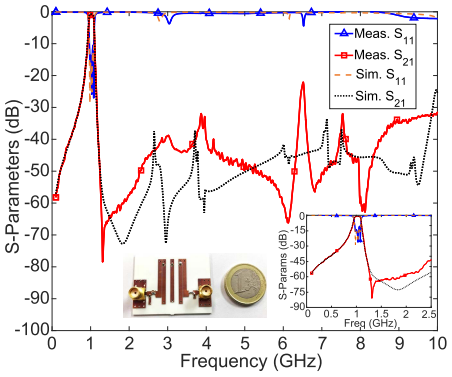

Fig. 5. Photography, measurements and simulation of the fabricated filter.

V. CONCLUSION

A general technique for implementing bandpass filters with ultra-wide stopband has been proposed in this letter, based on the introduction of TZs using lumped bisected $\pi-$sections and including the intrinsic parasitic elements of the discrete components. A filter example obtaining more than 22 dB of rejection up to $10 \times f_0$ has been designed and manufactured, showing an excellent agreement with the simulated results. This technique is general and can be applied to any filter in planar technology for improving the out-of-band response.

REFERENCES

[1] C. Quendo, E. Rius, C. Person, and M. Ney, "Integration of optimized low-pass filters in a bandpass filter for out-of-band improvement," *IEEE Trans. Microw. Theory Techn.*, vol. 49, no. 12, pp. 2376–2383, Dec. 2001.

[2] T. Lopetegi *et al.*, "Microstrip 'wiggly-line' bandpass filters with multi-spurious rejection," *IEEE Microw. Wireless Compon. Lett.*, vol. 14, no. 11, pp. 531–533, Nov. 2004.

[3] W. M. Fathelbab and M. B. Steer, "Parallel-coupled line filters with enhanced stopband performances," *IEEE Trans. Microw. Theory Techn.*, vol. 53, no. 12, pp. 3774–3781, Dec. 2005.

[4] K.-W. Hsu, M.-J. Tsou, Y.-H. Tseng, and W.-H. Tu, "Wide-stopband bandpass filter with symmetrical loaded-stub resonators," in *IEEE Proc. Asia–Pacific Microw. Conf.*, Dec. 2011, pp. 1043–1046.

[5] M. A. Sanchez-Soriano, G. Torregrosa-Penalva, and E. Bronchalo, "Multispurious suppression in parallel-coupled line filters by means of coupling control," *IET Microw., Antennas Propag.*, vol. 6, no. 11, pp. 1269–1276, Jun. 2012.

[6] J. Xu, Y.-X. Ji, W. Wu, and C. Miao, "Design of miniaturized microstrip LPF and wideband BPF with ultra-wide stopband," *IEEE Microw. Wireless Compon. Lett.*, vol. 23, no. 8, pp. 397–399, Aug. 2013.

[7] L. Hepburn and J.-S. Hong, "Compact integrated lumped element LCP filter," *IEEE Microw. Wireless Compon. Lett.*, vol. 26, no. 1, pp. 19–21, Jan. 2016.